Journal Pre-proof

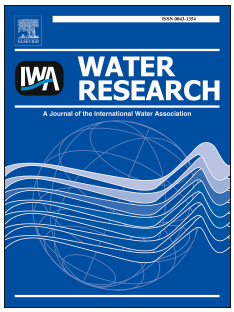

Photochemical transformation of perfluoroalkyl acid precursors in water using engineered nanomaterials

Yunrong Dai, Xingxing Guo, Siyu Wang, Lifeng Yin, Michael R. Hoffmann

PII: S0043-1354(20)30501-7

DOI: https://doi.org/10.1016/j.watres.2020.115964

Reference: WR 115964

To appear in: *Water Research*

Received Date: 20 December 2019

Revised Date: 14 May 2020

Accepted Date: 19 May 2020

Please cite this article as: Dai, Y., Guo, X., Wang, S., Yin, L., Hoffmann, M.R., Photochemical transformation of perfluoroalkyl acid precursors in water using engineered nanomaterials, *Water Research* (2020), doi: https://doi.org/10.1016/j.watres.2020.115964.


Industrial waste
PFAAs
Reactive oxygen radical
Engineered nanomaterials
PFAAs precuosr
Nano-polymer products

Photochemical Transformation of Perfluoroalkyl Acid Precursors in Water Using Engineered Nanomaterials

Yunrong Dai [a,b,*], *Xingxing Guo* [a], *Siyu Wang* [c], *Lifeng Yin* [b,d], *Michael R. Hoffmann* [b,*]

[a] School of Water Resources and Environment, Beijing Key Laboratory of Water Resources & Environmental Engineering, MOE Key Laboratory of Groundwater Circulation and Environmental Evolution, China University of Geosciences (Beijing), Beijing,100083, P. R. China

[b] Department of Environmental Science & Engineering, California Institute of Technology, Pasadena, CA 91125, United States

[c] Department of Urban Water Environmental Research, Basin Research Center for Water Pollution Control, Chinese Research Academy of Environmental Sciences, 100012, Beijing, P. R. China

[d] State Key Laboratory of Water Environment Simulation, School of Environment, Beijing Normal University, Beijing, 100875, P. R. China

Yunrong Dai, e-mail: daiyr@cugb.edu.cn

Xingxing Guo, e-mail: guoxx@cugb.edu.cn

Siyu Wang, e-mail: wangsy@craes.org.cn

Lifeng Yin, e-mail: lfyin@bnu.edu.cn

Michael R. Hoffmann, e-mail: mrh@caltech.edu

[*] Corresponding author. Tel. and fax: +86-10-82322281, +1-626-395-4391

E-mail: daiyr@cugb.edu.cn, daiyr@caltech.edu (Y. R. Dai), mrh@caltech.edu (M. R. Hoffmann)

Abstract

The production of perfluoroalkyl acids (PFAAs) has been phased out over recent decades; however, no significant decline in their environmental concentrations has been observed. This is partly due to the photochemical decomposition of PFAAs precursors (PrePFAAs) which remain in extensive use. The decomposition of PrePFAAs may be accelerated by the light-activated engineered nanomaterials (ENMs) in water. In light of this hypothesis, we investigated the photochemical transformation of three PrePFAAs, which are 8:2 fluorotelomer sulfonic acid (8:2 FTSA), 8:2 fluorotelomer alcohol (8:2 FTOH), and 2-(N-ethylperfluorooctane-1-sulfonamido ethyl] phosphate (SAmPAP), in the presence of six ENMs under simulated sunlight irradiation. The transformation rates of 8:2 FTSA and 8:2 FTOH were increased by 2–6 times when in the presence of six ENMs. However, most of ENMs appeared to inhibit the decomposition of SAmPAP. The transformation rates of PrePFAAs were found to depend on the yield of reactive oxygen species generated by ENMs, but the rates were also related to compound photo-stability, adsorption to surfaces, and photo-shielding effects. The PrePFAAs are transformed to perfluorooctanoic acid (PFOA) or/and perfluorooctane sulfonate (PFOS) with higher toxicity and longer half-life, PFOA or PFOS and a few PFAAs having shorter carbon chain lengths. Higher concentrations of the PFAAs photodegradation products were observed in the presence of most of the ENMs.

Keywords: PFAAs precursors, engineered nanoparticles, photochemical transformation, reactive oxygen species, PFOS, PFOA

1. Introduction

Perfluoroalkyl acids (PFAAs) are a class of poly- and perfluoroalkyl substances (PFASs) that have been used in thousands of products including Teflon cookware, pizza boxes, furniture, and clothing (Krafft and Riess, 2015). However, PFAAs are endocrine disrupters that have been shown to interfere with hormones, disrupt brain development in children, cause damage to male reproductive systems, and cause cancer (Grandjean and Clapp, 2014). The broad toxicity profile of PFAAs has led to their being gradually phased out of products in many countries since 2000; however, the concentrations of PFAAs in the environment are still relatively high (Gao et al., 2019, Gewurtz et al., 2019, Routti et al., 2016). This may be due to the decomposition of PFAA precursors (PrePFAAs) resulting in the formation of PFAAs (Nguyen et al., 2013, Peng et al., 2014).

PrePFAAs are produced either as industrial products or as chemical intermediates. Perfluorochemicals including perfluorooctylsulfonylfluoride (POSF) (Zhang et al., 2004), methyl perfluorooctane sulfonamide (MeFOSA) (Chu and Letcher, 2014), perfluorooctane sulfonamidoethanol (MeFOSE) (Avendano and Liu, 2015), *N*-ethyl perfluorooctane sulfonamide (EtFOSA), *N*-ethyl perfluorooctane sulfonamidoethanol (*N*-EtFOSE) (Gaillard et al., 2017) are used as precursors for the formation of perfluorinated sulfonic acids (PFSAs). Flourotelomer alcohols (PFOHs), perfluoroiodinealkanes (PFIs), perfluoroalkyl phosphates (PAPs), perfluorophosphonates (PFPAs), and perfluorophosphinates (PFPiAs) are used as precursors for the formation of perfluorinated carboxylic acids (PFCAs) (De Silva et al., 2012, Lee et al., 2012, Lee and Mabury, 2011). In addition, PrePFAAs are produced in quantities considerably larger than the quantified mass emissions of PFAAs (Houtz et al., 2013). PrePFAAs have been detected in rivers, lakes, sediments, wastewater treatment plant (WWTP)

effluents, and other environments (Chen et al., 2019, Gebbink et al., 2016, Schaefer et al., 2018, Wang et al., 2015).

In the environment, the transformations from most PrePFAAs to PFAAs proceed slowly with typical half-lives of 300 days (Liu and Avendano, 2013, Royer et al., 2015, Zhang et al., 2017). Many PrePFAAs are highly resistant to microbial degradation with little measured losses and/or associated product formation after 120 days (Avendano and Liu, 2015, Benskin et al., 2013, Dasu and Lee, 2016). For example, the SAmPAP diester was found to be recalcitrant with respect to microbial degradation after 120 days of incubation resulting in an estimated half-life of >380 days at 25 °C (Benskin et al., 2013). Photochemical transformation of PrePFAAs are quite slow given that most PrePFAAs lack of conjugated structures with very low sunlight molar extinction coefficients. Thus, the direct photochemical transformation of most PrePFAAs is unlikely to occur under ambient sunlight (Martin et al., 2006).

Both PrePFAAs and engineered nanomaterials (ENMs) are often used additives in synthetic fibers, rubbers, paints, dyes, paper products, cosmetics, and packing materials. For example Nanoclays combined with EtFOSE-based phosphate diester (e.g., SAmPAP diester) have been added to packaging materials in order to improve overall material strength, coating stability, and liquid or gas barrier properties (SCRCAP, 2014). Mixtures of nanoparticles with perfluorocarbons are used to prevent oxygen and water from penetrating through packaging containers (Geueke, 2016). Paper mills often add 0.1%–0.3% of nano-sized TiO_2, ZnO, or Fe_2O_3 to paper pulp for antistatic capacity and wear resistance coupled with perfluoroalkylethyl acrylate (trademark PF-001) for water and oil resistance. With the widespread use of ENMs coupled with PrePFAAs in commercial products, large quantities of ENMs and PrePFAAs are eventually released into the aquatic environment. Since many of the

commercially produced metal-oxide nanomaterials are photo-activated under UV-vis light coupled with bandgap energies ranging from 2.2 eV (530 nm) to 3.2 eV (385 nm), they are able to generate reactive oxygen species (ROS) including hydroxyl radical ($^{\bullet}OH$), superoxide anion ($O_2^{\bullet-}$), and singlet oxygen ($^1O_2$) under ambient sunlight irradiation (Buchman et al., 2019, Ganguly et al., 2018, Hoffmann et al., 1995). Thus the ENMs may be capable of producing indirect photochemical transformation of PrePFAAs in water leading to the formation of PFAAs as unintended byproducts. Previous studies have demonstrated that PrePFAAs are a source of PFAAs, but their photochemical transformation pathways are not resolved, and the photocatalytic impact of various ENMs on the transformation from PrePFAAs to PFAAs has little attention (Ahrens and Bundschuh, 2014, Sznajder-Katarzynska et al., 2019).

In light of the above concerns, we herein investigate the photochemical transformations of three typical PrePFAAs including 8:2 fluorotelomer sulfonic acid (8:2 FTSA), 8:2 fluorotelomer alcohol (8:2 FTOH), and 2-(N-ethylperfluorooctane-1-sulfonamido) ethyl phosphate (SAmPAP) under simulated sunlight irradiation in the presence of six different ENMs including TiO_2, ZnO, Fe_2O_3, CuO, graphene oxide (GO), and multi-walled carbon nanotubes (MWCNTs) in water. The effects of ENMs on the photolysis kinetics of PrePFAAs were examined. Meanwhile, photo-absorption, photo-shielding, ROS free radicals and band structure of six ENMs are analyzed to discuss the effects of ENMs on the transformation rates of PrePFAAs. In addition, the distribution and concentration levels of intermediate products are also detected during the photochemical transformation of PrePFAAs.

2. Materials and Methods

2.1 *Chemicals and Reagents*

8:2 fluorotelomer sulfonic acid (8:2 FTSA, $C_{10}H_5F_{17}SO_3$, 90%) was supplied by Synica Company (Shanghai, CHN). 8:2 fluorotelomer alcohol (8:2 FTOH, $C_{10}H_5F_{21}O$, 92%) was obtained from DuPont Specialty Chemicals (Delaware, USA). 2-(N-ethylperfluorooctane-1-sulfonamido) ethyl phosphate (SAmPAP, $C_{27}H_{25}F_{34}N_2O_8PS_2$, 90%) was purchased from Silworld Chemical Co., Ltd (Wuhan, CHN). All other PFAAs standard samples were supplied by Wellington Laboratories (Guelph, CA). Commercial nanomaterials, titanium dioxide (TiO_2), zinc oxide (ZnO), ferric oxide (Fe_2O_3), copper oxide (CuO), graphene oxide (GO), and hydroxyl group functionalized multi-walled carbon nanotubes (MWCNTs,) were purchased from Sigma-Aldrich (USA). All other chemicals used were of analytical grade. Deionized water (18.2 MΩ cm^{-1}) was obtained using a Milli-Q water purification system.

2.2 *Analysis and Characterization*

X-ray diffraction (XRD) was carried out using a D/MAX-2000 diffractometer (Rigaku, Japan) using Cu-Kα radiation at a scan rate (2θ) of 4° min^{-1} to determine the phase identity of the ENMs and the crystallite sizes. Fourier transform infrared (FTIR) spectroscopy was carried out at 400–4000 cm^{-1} on a Perkin-Elmer spectrometer (Spectrum 400, United States). Field emission scanning electron microscopy (FESEM, S4800, Hitachi, Japan) was employed for surface topography analysis. The particles size of ENMs was analyzed by Nanoparticle Size Analyzer (Nicoma 380, PSS, USA). A full-automatic specific surface area analyzer (ASAP 2020, Micrometrics, USA) was used to measure the specific surface area of ENMs. All the above characterizations are shown in Fig. S1–S4 and Table S1. Diffusion reflection spectroscopy (DRS) and UV-vis absorption spectroscopy were carried out on a Cary 500 UV-Vis NIR spectrophotometer (Agilent/Varian, USA) with an integrating sphere attachment in the

200–800 nm range. Teflon powder was employed as a reference. Electron paramagnetic resonance (EPR) spectra were collected on an EPR spectrometer (A300, Bruker, Germany) for radical analysis with DMPO and TEMP as the radical scavenger. DMPO was used as a trapping agent to characterize $^{\bullet}OH$ and $O_2^{\bullet-}$, and TEMP was used to trap $^1O_2$. The detailed measurement methods were shown in *Supplementary data*.

2.3 *Steady-State Photolysis Experiments*

Steady-state photochemical experiments were conducted to investigate the photochemical transformation of PrePFAAs and their intermediate products. The photochemical reactor vessel was constructed of a quartz glass cooling sleeve (250 mm high, 55 mm diameter) containing a quartz tube (25 mm external diameter) and sealed at one end. The tube was fitted in the reactor center with a Xenon lamp (CHF-XM-500W; Trusttech, China) with AM 1.5G filter to simulate sunlight. The actual photon flux was 1.7×10^{-10} ein s^{-1} cm^{-2}. The system temperature was controlled at 25±1°C by circulating water from a thermostatic water bath (VIVO Itherm-B3; Hamburg, Germany). PrePFAAs and ENM concentrations of 10 mg L^{-1} and 0.1 g L^{-1} were employed, respectively. PrePFAAs aqueous solutions were made from an acetone stock and phosphate buffer (pH=7.0±0.1, degassing with nitrogen). Prior to irradiation, the samples containing ENMs and PrePFAAs were exposed to the dark for 30 min under stirring (160 rpm) to establish an adsorption-desorption equilibrium. Then the Xenon lamp was initiated to conduct the photolytic experiments. The experiments were carried out over 8 h, with a sampling interval of 2 h and a sampling volume of 1 mL. To avoid the adsorption of PrePFAAs and their intermediate products on the ENMs and the vessels, each sampled reaction solution was firstly centrifuged (12,000 rpm) for 10 min to separate the liquid (ca. 1 mL of aqueous solution containing PrePFAAs and intermediates) and the solids

(ENMs), and then the ENMs was eluted with 1 mL of acetone at vortex mixer (800 rpm) for 10 min to elute the organic fluorine components. The obtained acetone supernatant (1 mL) was mixed with the aqueous solution (1 mL) to integrate an acetone-water mixture which was then concentrated into 100 μL by the rotary evaporation. The 100 μL of concentrated solution was injected into the HPLC-ESI-MS/MS for the further quantitative measure. Control experiments, i.e., in the absence of irradiation or ENMs, were conducted simultaneously. Experimental uncertainties evaluated in reactor without ENMs and irradiation were less than 5% of the initial concentrations. All experiments were carried out in triplicate, and the average value was adopted.

2.4 *Identification of Intermediates*

The concentrations of PrePFAAs and their intermediates in the photolysis reactions were monitored using a high-performance liquid chromatography electrospray ionization mass spectrometry system (HPLC-ESI-MS/MS; AB3200, Applied Biosystems, USA) equipped with a Symmetry C18 column. The electrospray ionization (ESI) source was operated in negative mode. A linear gradient of acetonitrile and 10 mmol L^{-1} of ammonium acetate aqueous solution (100:0 to 50:50) at a flow rate of 1.0 mL min^{-1} was used to separate the PrePFAAs and their intermediates over a total analysis time of 35 min. The products were identified using the MS/MS mode and were analyzed by multiple reaction monitoring (MRM) using their characteristic ion pairs (Table S2), and some identified products were also proofed by standard samples.

3. Results and Discussion

3.1 *Photo-absorption response*

The three PrePFAAs do not absorb light in the visible, however, there is a small amount of

UV light absorption below 300 nm. As shown in Fig. 1a, SAmPAP has the strongest absorption in the UV region, and its optimal tropospheric absorption overlap should occur at 295 nm. The absorption overlap for 8:2 FTOH is blue shifted by 5 nm down to the tropospheric cutoff of 290 nm for solar photochemistry. However, the UV absorption spectrum of 8:2 FTSA shows absorption only below 260 nm.

Fig. 1 here

The recorded DRS of the six ENMs are shown in Fig. 1b, where $nTiO_2$ and nZnO exhibit high photo-absorption in the UV region but no characteristic absorption in the visible light region (>400 nm), while nFe_2O_3 and nCuO both have stronger adsorption at longer wavelengths up to 600 nm. The absorption peaks of GO and MWCNTs are mainly in the UV region and their longer wavelength absorption is weak. These ENMs can absorb the simulated sunlight and undergo bandgap excitation, which might bridge the light irradiation and photochemical reaction of PrePFAAs in aqueous solutions. In some cases, these ENMs had photo-shielding effects (see Fig. S7) due to nanoparticles floating on the surface of water resulting in light scattering and surface refraction of incident light leading to reduced direct or indirect photolysis of the PrePFAAs. Therefore, the co-existence of ENMs and PrePFAAs in water body has the potential to influence photochemical transformations of the PrePFAAs.

3.2 *Transformation Kinetics of three PrePFAAs*

Fig. 2 and Table S3 summarize the observed photolysis kinetics of the three target PrePFAAs under simulated sunlight irradiation. The disappearance of the three PrePFAAs followed apparent first-order reaction kinetics with the corresponding photolytic rates of

0.069 h^{-1}, 0.148 h^{-1}, and 0.890 h^{-1} for 8:2 FTSA, 8:2 FTOH, and SAmPAP, respectively. Since there is a small intersection between the simulated solar spectrum and the absorption spectra of SAmPAP or 8:2 FTOH, (see Fig. 1 inset), indicating that SAmPAP and 8:2 FTOH might be transformed via the direct photolysis. However, there is no intersection between the simulated solar spectrum and 8:2 FTSA, thus 8:2 FTSA is not likely to be decomposed under sunlight. Furthermore, the frontier molecular orbitals (FMO) analysis results for the three PrePFAAs also indicate that the stability of SAMPAP is less than those of 8:2 FTSA and 8:2 FTOH (see Fig. S8). The FMO prediction is consistent with the observed faster transformation rate of SAMPAP during the direct photolysis process.

Fig. 2. here

Significant differences were observed during the PrePFAAs photolysis in the presence of the ENMs. Under simulated sunlight irradiation, the photolytic rates of 8:2 FTSA and 8:2 FTOH were increased by about 2–6 times in the presence of six ENMs. nTiO_2 had the most significant enhancement effect on the transformation of 8:2 FTSA and 8:2 FTOH in which the first-order rate constants for photolysis increased from 0.069 h^{-1} and 0.148 h^{-1} to 0.416 h^{-1} and 0.812 h^{-1}, respectively. In the case of nZnO, the photolytic rate constant of 8:2 FTOH was higher than those observed for nFe_2O_3, nCuO, GO and MWCNTs. However, it had the lowest first-order photolysis rate constant for the transformation of 8:2 FTSA. Even though the photo absorptivity of nFe_2O_3 is much higher than that of nCuO, the photolysis rate constants for 8:2 FTSA and 8:2 FTOH were somewhat lower than those observed for nCuO. The photolysis rate constants for 8:2 FTSA and 8:2 FTOH were moderately enhanced by GO and MWCNTs. By contrast, the enhancement effects of ENMs on the photolysis of 8:2 FTSA and 8:2 FTOH

in water could be higher than that of dissolved organic matter (DOM) under the same concentration (see *Supplementary data*). However, the photolytic rate constants for SAmPAP was not enhanced in the presence of $nTiO_2$. Moreover, they were decreased substantially in the presence of nFe_2O_3, nCuO, GO and MWCNTs. For example, in a suspension of nFe_2O_3 photolysis rate constant for SAmPAP decreased by factor of 6.7. It is clear in this specific case, that hematite nanoparticles inhibit the photolytic degradation of SAmPAP in water. In contrast, the relative inhibition effects of nCuO, GO and MWCNTs on the photolytic transformation of SAmPAP were minor.

3.3 *Free Radicals and Band Structure Analyses*

In the case of PrePFAAs coexisting with ENMs, indirect photolysis by the photo-generated ROS of ENMs, such as $^{\bullet}OH$, $O_2^{\bullet-}$, and $^1O_2$, may play an important role in the transformation of PrePFAAs. The standard state redox potential (E_H) of the dissolved oxygen/superoxide anion pair ($O_2/O_2^{\bullet-}$), singlet oxygen/dissolved oxygen pair ($^1O_2/O_2$) and water/hydroxyl radical pair ($H_2O/^{\bullet}OH$) in aqueous solution is –0.20, 1.88, and 2.20 eV, respectively (Li et al., 2012). Theoretically, in order to generate $O_2^{\bullet-}$, the potential of the photo-generated electrons of the material should be lower than –0.20 eV, so that there is sufficient reducing capacity to reduce O_2 to $O_2^{\bullet-}$. Similarly, if $^1O_2$ and $^{\bullet}OH$ are formed in the photolytic system involving ENMs, then the potential of the photo-generated holes of the material should be greater than 1.88 eV and 2.20 eV, respectively, so that there is enough energy to oxidize H_2O (OH^-) to $^{\bullet}OH$ and to excite ground state $^3O_2$ to $^1O_2$.

Fig. 3 shows the EPR spectra of DMPO/$^{\bullet}OH$, DMPO/$O_2^{\bullet-}$, and TEMP/$^1O^2$ adducts produced by different ENMs under simulated sunlight irradiation. There is no EPR signal in the DMPO and DMPO-ENMs hybrid systems in the absence of irradiation. After irradiation,

the DMPO and ENMs ($nTiO_2$, nZnO, nCuO, GO) hybrid system have a characteristic peak of 1:2:2:1 (Fig. 3a), which is the DMPO/$^{\bullet}$OH adduct formed by the reaction of DMPO with $^{\bullet}$OH. It can be seen from Fig. S9 that the valence band potentials (E_v) values of four metal-oxide ENMs, $nTiO_2$ (2.92 eV), nZnO (3.08 eV), nCuO (2.39 eV) and nFe_2O_3 (2.66 eV) are higher than the E_H of $H_2O/^{\bullet}OH$ (2.20 eV) and $^1O_2/^3O_2$ (1.88 eV) (Li et al., 2012). Thus, the holes generated by these ENMs can oxidize H_2O to $^{\bullet}$OH and excite $^3O_2$ to $^1O_2$, respectively. However, the $^{\bullet}$OH and $^1O_2$ were not detected in the nFe_2O_3 suspension. This probably because the recombination rate of electrons and holes generated by the α-Fe_2O_3 ENMs is high, and the diffusion lengths of holes are also low (2–4 nm), which requires a larger potential for the photo-assisted water oxidation by α-Fe_2O_3 (Mishra and Chun, 2015). As shown in Fig. 4, the concentrations of $^{\bullet}$OH and $^1O_2$ generated by nZnO are significantly higher than those obtained with $nTiO_2$, especially the yield of $^{\bullet}$OH in nZnO was approximately 3-fold more than that in $nTiO_2$, which is consistent with previous reports (Wang et al., 2017). This probably because the E_v of nZnO is higher due to quantum sizing effects than comparable shifts for $nTiO_2$. In addition, considering the much stronger bonding energy of Ti-O (666.5 kJ/mol) than Zn-O (250 kJ/mol), surface bound hydroxyl radicals may disassociate more difficultly from TiO_2 than that from ZnO, resulting in lower concentration of hydroxyl radicals in solution, and may be less likely to form DMPO adducts (Haynes, 2009). The E_c value of $nTiO_2$ (–0.28 eV) is lower than the E_H of $O_2/O_2^{\bullet-}$ (–0.20 eV), indicating that the potential of $nTiO_2$ to generate $O_2^{\bullet-}$, which agrees with the experimental result shown in Fig. 3. Unexpectedly, considerable amount of $O_2^{\bullet-}$ could also been detected in the nZnO and nCuO suspensions, although their E_c values (–0.12 and 0.69 eV, respectively) are higher than –0.20 eV. For nZnO, the actual E_c may be lower than −0.20 eV due to quantum sizing effects, allowing electron transfer from

the conduction band to O_2 molecules and generating $O_2^{\bullet-}$ (Li et al., 2012, Wang et al., 2017). For CuO, it has been reported that the significant quantity of superoxide anions might be rendered directly from the surface defect sites (such as Cu(I) sites) in nanocrystalline CuO (Meghana et al., 2015). Even though nFe_2O_3 is n-type semiconductor, it did not produce $O_2^{\bullet-}$, or the concentrations were below the detection limit. This may be due the considerable difference between the E_c of nFe_2O_3 (0.46 eV) and the E_H of $O_2/O_2^{\bullet-}$.

Fig. 3. here

Fig. 4. here

For the two carbon nanomaterials, $O_2^{\bullet-}$ and $^1O_2$ signals were detected. The MWCNTs suspension gave stronger adduct signals, while the GO suspension gave weaker $^{\bullet}OH$ and $^1O_2$ signals. As a one-dimensional nano-material with excellent electrical properties, CNTs have a band gap determined by the circumferential quantum confinement, which depends on the diameter and chirality. The band gap of MWCNTs ranged from 23 meV to 2.7 eV depending on the radial deformation (Gelao et al., 2019). Similarly, the GO can be regarded as an unfolded CNT with similar electronic structures. However, the abundance of –COOH, –OH, and $–SO_3H$ functional groups and defects on edge of GO nanostructure results in variable band gap energies from zero (metallic) to 6.5 eV (Lundie et al., 2014). Thus, it is difficult to estimate whether they can generate ROS by using their E_v and E_c values. It is reported that types of surface functionalization, defects on the surface, as well as differences in amorphous carbon and metal impurity content during preparations (e.g., Fe), may facilitate the photo-generation of some ROS by CNTs or GO (Chen and Jafvert, 2011, Felip-Leon et al.,

2019, Qu et al., 2013, Zhao and Jafvert, 2015). Carboxylate and hydroxylated MWCNTs have been proved to produce ROS, which agree with our experimental result that MWCNTs with –OH groups produced $O_2^{\bullet-}$ and $^1O_2$. The numerous functional groups and defect sites on the surface of GO may lead to the formation of $^{\bullet}OH$ and $^1O_2$.

The indirect photochemical transformation rates of PrePFAAs depend on the ROS yields generated by ENMs, but they are also related to their intrinsic stability, surface sorption ability, and photo-shielding effects. The enhancement effects for most of ENMs in the case of 8:2 FTSA and 8:2 FTOH are positively correlated with the ROS concentrations that are generated except for nZnO. As mentioned above, the yield of $^{\bullet}OH$ and $^1O_2$ generated by nZnO are higher than for the other ENMs. If the transformation of the PrePFAAs in the presence of the ENMs are controlled only by ROS yield, then nZnO should accelerate the transformation rates of the PrePFAAs more than other ENMs. In contrast to this prediction, however, the photolytic transformation rates of 8:2 FTSA and 8:2 FTOH were the fastest in the presence of $nTiO_2$. On one hand, $nTiO_2$ is an active photocatalyst at $\lambda < 385$ nm that produces ROS. On the other hand, nZnO particles are relatively unstable with respect to reversion to $Zn(OH)_2$. In addition, nZnO photo-corrosion during irradiation time >1.0 h may reduce the apparent photocatalytic activity (Hoffmann et al., 1995, Okamoto et al., 1985, Zhang et al., 2009) when compared to much short irradiation time. The high ROS concentrations measured during our experiments with nZnO were detected after 10-minute of irradiation. Photo-corrosion may not have had a significant impact during this relatively short irradiation time. However, the ROS yields with nZnO may be lower during an 8 h illumination time due to the accumulative effects of photo-corrosion. The photolytic decomposition rates of 8:2 FTSA and 8:2 FTOH in suspensions of GO were found to be slightly higher than those measured with MWCNTs,

318 which might be attributed to the relatively stronger oxidation capacity of ·OH generated by
319 GO.

320 In the case of SAMPAP, direct photolysis results in its relatively rapid decomposition,
321 which is most likely due to its lack of chemical stability. As a result, the proportional
322 contribution of ROS produced by the ENMs to the transformation of SAmPAP is not obvious.
323 The SAmPAP transformation rates in the presence of $nTiO_2$ and nZnO were comparable to the
324 measured direct photolysis rate, whereas in the presence of CuO, GO and MWCNTs were
325 clearly lower than the corresponding direct photolysis rate. That is because the ROS yield
326 might counteract the photo-shielding effects of colloidal ENMs entirely or partly. However,
327 the SAmPAP transformation rate in suspensions of nFe_2O_3 were decreased dramatically.
328 This effect can be attributed to the lack ROS detected in the nFe_2O_3 suspensions as a counter
329 balance to the photo-shielding effects.

330 **3.4** ***Intermediate Products***

331 It is known that PrePFAAs undergo defluorination, hydrolysis, β-oxidation, and enzymatic
332 reactions to produce various PFAAs that have different degrees of toxicity and ecological
333 risks in the aqueous environment and to aquatic and terrestrial organisms (Appleman et al.,
334 2014, Houtz et al., 2016). The PFAAs transformed from PrePFAAs mainly include PFCAs
335 and PFSAs with different carbon chain lengths. Perfluorooctanoic acid (PFOA) and
336 perfluorooctane sulfonate (PFOS) are the most studied PFCAs and PFSAs, respectively. Both
337 of them are PFAAs with long carbon chain (C8), and are main decomposition products of
338 many PrePFAAs (Gebbink et al., 2016). In the present study, some of PFCAs and PFSAs with
339 different carbon chain lengths (C_4-C_8) have been detected by LC-ESI-MS/MS as intermediate
340 reaction products during photolysis of the PrePFAAs as summarized in Table S2. The carbon

and fluorine recovery rates were analyzed, and the high fluorine recovery rates (mainly in the range of 56%~98%) indicate that it is sufficient to clarify the photochemical transformation of the three PrePFAAs based on the detected intermediates (see *Supplementary data*).

Since the PrePFAAs samples used in this study were commercial industrial-grade products, various intermediate PFCAs and PFSAs products were detected at measurable concentrations in the stock solutions of the PrePFAAs. Therefore, the increase in concentration during photolysis relative to the initial concentration was used to determine the production of the intermediate reaction products. Based on this approach, SAmPAP was found to be transformed into both PFCAs and PFSAs, although the concentrations of PFCAs were found to be much higher than the concentrations of the PFSAs (see Fig. 5). Furthermore, the concentrations of both PFCAs and PFSAs with longer carbon chain, such as PFOA and PFOS, were higher than that those with relatively shorter carbon chain, such as PFPnA, PFBA, PFPnS and PFBS. In contrast, 8:2 FTSA and 8:2 FTOH were decomposed only into PFCAs with the concentrations of the longer carbon chain PFCAs higher than those of shorter carbon chain products. For comparison, after sunlight irradiation for 8 h, the PFOA formed by photolysis of SAmPAP was more than 10 times higher than that formed from 8:2 FTSA, and more than 20 times higher than that formed from 8:2 FTOH photolysis. Thus, it is clear that all three PrePFAAs can be photolytically transformed into PFCAs and/or PFSAs of different carbon chain lengths (C_4-C_8) under simulated sunlight irradiation conditions, and the C8 products, PFOA or PFOS, were found to be the main products.

Fig. 5. here

When photo-activated ENMs are present with PrePFAAs in a body of water, they will affect not only the photolytic transformation rates of PrePFAAs, but also the generation rates and concentrations of the various intermediate reaction products. For instance, with $nTiO_2$, the photolytic efficiencies of 8:2 FTSA and 8:2 FTOH were enhanced under simulated sunlight irradiation and more PFCAs were detected in the reaction solution. The concentration of PFOA formed from 8:2 FTSA was over 2 times higher than that without $nTiO_2$. During photolysis of 8:2 FTOH with $nTiO_2$, similar concentration of PFOA were produced. However, the concentrations of PFHpA and PFHxA were increased by three orders of magnitude, and the concentrations of PFPnA and PFBA were also increased by one or two orders of magnitude. In addition, PFCAs with different carbon chains (C_4-C_8) were detected in the SAmPAP/$nTiO_2$ reaction solution with concentrations in the range of 10^2 to 10^3 nmol L^{-1}. These concentrations were about 30 times higher than those in measured in the absence of $nTiO_2$. Thus, it is clear that photolysis of suspensions of 8:2 FTOH or SAmPAP with $nTiO_2$ in water under sunlight irradiation readily form PFCA. Similar results were observed in suspensions of 8:2 FTOH or SAmPAP with ZnO. When the 8:2 FTSA or 8:2 FTOH were irradiated in suspensions of Fe_2O_3, CuO, GO or MWCNTs, the final concentrations of most reaction products were similar, although their rates of production were different in the case of each ENM.

Although the photolytic transformation rates for SAmPAP in the presence of the ENMs were much lower compared to photolysis in the absence of the ENMs (as shown in Fig. 2), the steady-state concentrations of the intermediate products found to be just slightly lower than those detected during photolysis in the absence of ENMs. Since SAmPAP has a 27 backbone combined with 34 fluorines, there are clearly multiple steps involved leading to the

formation of PFOA, PFOS, and related PFAAs having carbon chains ≤ C8 (see Fig. S12). The initial transformations must involve multiple steps in order for the parent C27 molecule to be cleaved into PFAAs with carbon numbers >C8. The ENMs did not appear to inhibit rates of production or steady-state concentrations of C4 to C8 PFAAs that were detected. In some cases, the detected C4 and C5 PFCAs and PFCSs concentrations declined with the increase of photolysis time, which may be due to the photocatalytic impact of the ENMs.

4. Conclusions

In the present study, the photochemical transformation processes of three typical PrePFAAs in the presence of six ENMs under simulated sunlight irradiation were investigated. Based on our investigation, it is clear that the transformation of PrePFAAs into PFAAs is influenced by the photochemical activity of the studied ENMs. The direct photolysis rates of 8:2 FTSA and 8:2 FTOH are found to be low, but photolytic conversion of SAmPAP is relatively facile. Furthermore, in suspensions of $nTiO_2$, nZnO, nFe_2O_3, nCuO, GO and MWCNTs, the transformation rates of 8:2 FTSA and 8:2 FTOH were enhanced under simulated sunlight irradiation, while most of ENMs had inhibiting effects on the photolysis of SAmPAP. Photo-generated ROS on the surfaces of the ENMs play a key role in PrePFAAs decomposition. In addition, the photochemical transformation of PrePFAAs might be also related to the photo-stability, adsorption to surfaces, and photo-shielding effects. Meanwhile, these PrePFAAs could be transformed to PFOA or PFOS or other PFAAs products, and higher concentrations of PFAAs products were detected in the presence of most ENMs.

Indeed, both the PrePFAAs and ENMs are widely used together in various industrial and commercial applications. With the rapid development of nanotechnology, the number of PrePFAAs/ENMs-containing industrial products on the market has increased. The PrePFAAs

and ENMs containing products are eventually released into the environment, and inevitably exposed to sunlight. The inherent photochemical properties of many ENMs will most likely affect the transport and transformation of PrePFAAs in water. Nevertheless, in the ambient water environment, various photolysis reactions may be more complicated due the various competing reaction pathways including the photoactivity of DOM, sorption to organic surfaces, biodegradation, and loss to the sediments. Meanwhile, the acceleration or inhibition effects of ENMs might be also influenced by the efficiency limitation of mass transfer, radical quenching or more complex components in the actual water environment. Anyway, when the PrePFAAs coexist with ENMs in water, part of these ENMs could accelerate the transformation from PrePFAAs to PFOA or/and PFOS with higher toxicity and longer half-life. Therefore, it is necessary to pay more attention to the photochemical transformation behavior of PrePFAAs coexisting with ENMs in water, and also focus more on the influence of actual environmental factors next.

Declaration of competing interest

The authors declare that they have no known competing financial interests or personal relationships that could have appeared to influence the work reported in this paper.

Acknowledgments

This work was financially supported by the National Key R&D Program of China (2018YFC1800400), the National Natural Science Foundation of China (Project 21777009 and 21407138), the Beijing Municipal Natural Science Foundation (8182031), and the

Fundamental Research Funds for the Central Universities of China (649911019). The authors would like to thank Engineer Wang from Shiyanjia Lab (www.shiyanjia.com) for the EPR analysis.

Appendix A. Supplementary data

Supplementary data related to this article can be found at http://dx.doi.org/10.1016/j.watres.....

References

Stockholm convention regional centre for capacity-building and the transfer of technology in Asia and the Pacific (SCRCAP), 2014. POPs in articles and phasing-out opportunities, Beijing, China.

Ahrens, L. and Bundschuh, M., 2014. Fate and effects of poly- and perfluoroalkyl substances in the aquatic environment: A review. Environ. Toxicol. Chem. 33(9), 1921-1929. https://doi.org/10.1002/etc.2663.

Appleman, T.D., Higgins, C.P., Quinones, O., Vanderford, B.J., Kolstad, C., Zeigler-Holady, J.C. and Dickenson, E.R.V., 2014. Treatment of poly- and perfluoroalkyl substances in US full-scale water treatment systems. Water Res. 51, 246-255. https://doi.org/10.1016/j.watres.2013.10.067.

Avendano, S.M. and Liu, J.X., 2015. Production of PFOS from aerobic soil biotransformation of two perfluoroalkyl sulfonamide derivatives. Chemosphere 119, 1084-1090. http://doi.org/10.1016/j.chemosphere.2014.09.059.

Benskin, J.P., Ikonomou, M.G., Gobas, F.A.P.C., Begley, T.H., Woudneh, M.B. and Cosgrove, J.R., 2013. Biodegradation of N-ethyl perfluorooctane sulfonamido ethanol (EtFOSE) and EtFOSE-based phosphate diester (SAmPAP Diester) in marine sediments. Environ. Sci. Technol. 47(3), 1381-1389.

https://doi.org/10.1021/es304336r.

Buchman, J.T., Hudson-Smith, N.V., Landy, K.M. and Haynes, C.L., 2019. Understanding nanoparticle toxicity mechanisms to inform redesign strategies to reduce environmental impact. Acc. Chem. Res. 52(6), 1632-1642. https://doi.org/10.1021/acs.accounts.9b00053.

Sinograce Chemical, 2015. PF-001 is perfluoroalkylethyl acrylate used for treating surfaces to impart oil resistance, water resistance and stain resistance. https://www.sinogracechem.com/perfluoroalkylethyl-acrylate-pf-001_p82.html

Chen, C.-Y. and Jafvert, C.T., 2011. The role of surface functionalization in the solar light-induced production of reactive oxygen species by single-walled carbon nanotubes in water. Carbon 49(15), 5099-5106. https://doi.org/10.1016/j.carbon.2011.07.029.

Chen, H., Zhang, L., Li, M., Yao, Y., Zhao, Z., Munoz, G. and Sun, H., 2019. Per- and polyfluoroalkyl substances (PFASs) in precipitation from mainland China: Contributions of unknown precursors and short-chain (C2-C3) perfluoroalkyl carboxylic acids. Water Res. 153, 169-177. https://doi.org/10.1016/j.watres.2019.01.019.

Chu, S.G. and Letcher, R.J., 2014. In vitro metabolic formation of perfluoroalkyl sulfonamides from copolymer surfactants of pre- and post-2002 scotchgard fabric protector products. Environ. Sci. Technol. 48(11), 6184-6191. http://doi.org/10.1021/es500169x.

Dasu, K. and Lee, L.S., 2016. Aerobic biodegradation of toluene-2,4-di(8:2 fluorotelomer urethane) and hexamethylene-1,6-di(8:2 fluorotelomer urethane) monomers in soils. Chemosphere 144, 2482-2488. https://doi.org/10.1016/j.chemosphere.2015.11.021.

De Silva, A.O., Allard, C.N., Spencer, C., Webster, G.M. and Shoeib, M., 2012. Phosphorus-containing fluorinated organics: Polyfluoroalkyl phosphoric acid diesters (diPAPs), Perfluorophosphonates (PFPAs), and perfluorophosphinates (PFPIAs) in residential indoor dust. Environ. Sci. Technol. 46(22),

12575-12582. http://doi.org/10.1021/es303172p.

Felip-Leon, C., Puche, M., Miravet, J.F., Galindo, F. and Feliz, M., 2019. A spectroscopic study to assess the photogeneration of singlet oxygen by graphene oxide. Mater. Lett. 251, 45-51. https://doi.org/10.1016/j.matlet.2019.05.001.

Gaillard, J., Veyrand, B., Thomas, M., Dauchy, X., Boiteux, V., Marchand, P., Le Bizec, B., Banas, D. and Feidt, C., 2017. Tissue uptake, distribution, and elimination of perfluoroalkyl substances in juvenile perch through perfluorooctane sulfonamidoethanol based phosphate diester dietary exposure. Environ. Sci. Technol. 51(13), 7658-7666. http://doi.org/10.1021/acs.est.6b05598.

Ganguly, P., Breen, A. and Pillai, S.C., 2018. Toxicity of nanomaterials: Exposure, pathways, assessment, and recent advances. ACS Biomater. Sci. Eng. 4(7), 2237-2275. https://doi.org/10.1021/acsbiomaterials.8b00068.

Gao, Y., Liang, Y., Gao, K., Wang, Y., Wang, C., Fu, J., Wang, Y., Jiang, G. and Jiang, Y., 2019. Levels, spatial distribution and isomer profiles of perfluoroalkyl acids in soil, groundwater and tap water around a manufactory in China. Chemosphere 227, 305-314. http://doi.org/10.1016/j.chemosphere.2019.04.027.

Gebbink, W.A., Bignert, A. and Berger, U., 2016. Perfluoroalkyl acids (PFAAs) and selected precursors in the baltic sea environment: Do precursors play a role in food web accumulation of PFAAs? Environ. Sci. Technol. 50(12), 6354-6362. http://doi.org/10.1021/acs.est.6b01197.

Gelao, G., Marani, R. and Perri, A.G., 2019. A formula to determine energy band gap in semiconducting carbon nanotubes. ECS J. Solid State Sci. Technol. 8(2), M19-M21. https://doi.org/10.1149/2.0201902jss.

Geueke, B., 2016. FPF dossier: Per- and polyfluoroalkyl substances (PFASs). https://doi.org/10.5281/zenodo.57198.

Gewurtz, S.B., Bradley, L.E., Backus, S., Dove, A., McGoldrick, D., Hung, H. and Dryfhout-Clark, H., 2019. Perfluoroalkyl acids in great lakes precipitation and surface water (2006-2018) indicate response to phase-outs, regulatory action, and variability in fate and transport processes. Environ. Sci. Technol. 53(15), 8543-8552. http://doi.org/10.1021/acs.est.9b01337.

Grandjean P., Clapp R., 2014. Changing interpretation of human health risks from perfluorinated compounds. Public Health Rep. 129.

Haynes, W.M. (2009) CRC handbook of chemistry and physics: A ready-reference book of chemical and physical data, Boca Raton: CRC Press.

Hoffmann, M.R., Martin, S.T., Choi, W.Y. and Bahnemann, D.W., 1995. Environmental applications of semiconductor photocatalysis. Chem. Rev. 95(1), 69-96. https://doi.org/10.1021/cr00033a004.

Houtz, E.F., Higgins, C.P., Field, J.A. and Sedlak, D.L., 2013. Persistence of perfluoroalkyl acid precursors in AFFF-impacted groundwater and soil. Environ Sci Technol 47(15), 8187-8195. http://doi.org/10.1021/es4018877.

Houtz, E.F., Sutton, R., Park, J.S. and Sedlak, M., 2016. Poly- and perfluoroalkyl substances in wastewater: Significance of unknown precursors, manufacturing shifts, and likely AFFF impacts. Water Res. 95, 142-149. http://10.1016/j.watres.2016.02.055.

Krafft, M.P. and Riess, J.G., 2015. Selected physicochemical aspects of poly- and perfluoroalkylated substances relevant to performance, environment and sustainability-Part one. Chemosphere 129, 4-19. http://10.1016/j.chemosphere.2014.08.039.

Lee, H., De Siva, A.O. and Mabury, S.A., 2012. Dietary bioaccumulation of perfluorophosphonates and perfluorophosphinates in juvenile rainbow trout: Evidence of metabolism of perfluorophosphinates. Environ. Sci. Technol. 46(6), 3489-3497. http://doi.org/10.1021/es204533m.

Lee, H. and Mabury, S.A., 2011. A pilot survey of legacy and current commercial fluorinated chemicals in

525 human sera from United States donors in 2009. Environ. Sci. Technol. 45(19), 8067-8074.
526 http://doi.org/10.1021/es200167q.
527 Li, Y., Zhang, W., Niu, J. and Chen, Y., 2012. Mechanism of photogenerated reactive oxygen species and
528 correlation with the antibacterial properties of engineered metal-oxide nanoparticles. ACS Nano 6(6),
529 5164-5173. https://doi.org/10.1021/nn300934k.
530 Liu, J.X. and Avendano, S.M., 2013. Microbial degradation of polyfluoroalkyl chemicals in the
531 environment: A review. Environ. Int. 61, 98-114. https://doi.org/10.1016/j.envint.2013.08.022.
532 Lundie, M., Sljivancanin, Z. and Tomic, S. (2014) 4th Workshop on Theory, Modelling and Computational
533 Methods for Semiconductors. Pal, J., Migliorato, M. and Tomic, S. (eds).
534 Martin, J.W., Ellis, D.A., Mabury, S.A., Hurley, M.D. and Wallington, T.J., 2006. Atmospheric chemistry of
535 perfluoroalkanesulfonamides: Kinetic and product studies of the OH radical and Cl atom initiated
536 oxidation of N-ethyl perfluorobutanesulfonamide. Environ. Sci. Technol. 40(3), 864-872.
537 https://doi.org/10.1021/es051362f.
538 Meghana, S., Kabra, P., Chakraborty, S. and Padmavathy, N., 2015. Understanding the pathway of
539 antibacterial activity of copper oxide nanoparticles. RSC Advances 5(16), 12293-12299.
540 https://doi.org/10.1039/c4ra12163e.
541 Mishra, M. and Chun, D.M., 2015. Alpha-Fe_2O_3 as a photocatalytic material: A review. Applied Catalysis
542 A-General 498, 126-141. https://doi.org/10.1016/j.apcata.2015.03.023.
543 Nguyen, T.V., Reinhard, M. and Gin, K.Y.H., 2013. Rate laws and kinetic modeling of N-ethyl
544 perfluorooctane sulfonamidoethanol (N-EtFOSE) transformation by hydroxyl radical in aqueous
545 solution. Water Res. 47(7), 2241-2250. https://doi.org/10.1016/j.watres.2013.01.047
546 Okamoto, K., Yamamoto, Y., Tanaka, H., Tanaka, M. and Itaya, A., 1985. Heterogeneous photocatalytic
547 decomposition of phenol over TiO_2 powder. Bull. Chem. Soc. Jpn. 58(7), 2015-2022.

https://doi.org/10.1246/bcsj.58.2015.

Peng, H., Zhang, S., Sun, J., Zhang, Z., Giesy, J.P., Hu. J., 2014. Isomer-specific accumulation of perfluorooctanesulfonate from (N-ethyl perfluorooctanesulfonamido)ethanol-based phosphate diester in Japanese Medaka (Oryzias latipes). Environ. Sci. Technol. 48, (2), 1058-1066. https://doi.org/10.1021/es404867w

Qu, X., Alvarez, P.J.J. and Li, Q., 2013. Photochemical transformation of carboxylated multiwalled carbon nanotubes: Role of reactive oxygen species. Environ. Sci. Technol. 47(24), 14080-14088. https://doi.org/10.1021/es4033056.

Routti, H., Gabrielsen, G.W., Herzke, D., Kovacs, K.M. and Lydersen, C., 2016. Spatial and temporal trends in perfluoroalkyl substances (PFASs) in ringed seals (Pusa hispida) from Svalbard. Environ Pollut 214, 230-238. http://doi.org/10.1016/j.envpol.2016.04.016.

Royer, L.A., Lee, L.S., Russell, M.H., Nies, L.F. and Turco, R.F., 2015. Microbial transformation of 8:2 fluorotelomer acrylate and methacrylate in aerobic soils. Chemosphere 129, 54-61. https://doi.org/10.1016/j.chemosphere.2014.09.077.

Schaefer, C.E., Choyke, S., Ferguson, P.L., Andaya, C., Burant, A., Maizel, A., Strathmann, T.J. and Higgins, C.P., 2018. Electrochemical transformations of perfluoroalkyl acid (PFAA) precursors and PFAAs in groundwater impacted with aqueous film forming foams. Environ. Sci. Technol. 52(18), 10689-10697. http://doi.org/10.1021/acs.est.8b02726.

Sznajder-Katarzynska, K., Surma, M. and Cieslik, I., 2019. A review of perfluoroalkyl acids (PFAAs) in terms of sources, applications, human exposure, dietary intake, toxicity, legal regulation, and methods of determination. J. Chem-Ny. http://doi.org/10.1155/2019/2717528.

Wang, D., Zhao, L., Ma, H., Zhang, H. and Guo, L.-H., 2017. Quantitative analysis of reactive oxygen species photogenerated on metal oxide nanoparticles and their bacteria toxicity: The role of superoxide

radicals. Environ. Sci. Technol. 51(17), 10137-10145. https://doi.org/10.1021/acs.est.7b00473.

Wang, Z., Cousins, I.T., Scheringer, M. and Hungerbuehler, K., 2015. Hazard assessment of fluorinated alternatives to long-chain perfluoroalkyl acids (PFAAs) and their precursors: Status quo, ongoing challenges and possible solutions. Environ. Int. 75, 172-179. http://doi.org/10.1016/j.envint.2014.11.013.

Zhang, L., Cheng, H., Zong, R. and Zhu, Y., 2009. Photocorrosion suppression of ZnO nanoparticles via hybridization with graphite-like carbon and enhanced photocatalytic activity. J. Phys. Chem. C 113(6), 2368-2374. https://doi.org/10.1021/jp807778r.

Zhang, L.L., Lee, L.S., Niu, J.F. and Liu, J.X., 2017. Kinetic analysis of aerobic biotransformation pathways of a perfluorooctane sulfonate (PFOS) precursor in distinctly different soils. Environ. Pollut. 229, 159-167. https://doi.org/10.1016/j.envpol.2017.05.074.

Zhang, W., Nagashima, T., Lu, Y.M. and Chen, C.H.T., 2004. A traceless perfluorooctylsulfonyl tag for deoxygenation of phenols under microwave irradiation. Tetrahedron Lett. 45(24), 4611-4613. http://doi.org/10.1016/j.tetlet.2004.04.115.

Zhao, Y. and Jafvert, C.T., 2015. Environmental photochemistry of single layered graphene oxide in water. Environ. Science-Nano 2(2), 136-142. https://doi.org/10.1039/c4en00209a.

Figure captions

Fig. 1. (a) Molar absorptivity of 8:2 FTSA, 8:2 FTOH, SAmPAP, and emission spectra of simulated sunlight (Xenon lamp with AM 1.5G filter); (b) Diffuse reflection spectrum of six ENMs, including $nTiO_2$, nZnO, nFe_2O_3, nCuO, GO and MWCNTs.

Fig. 2. Transformation kinetics of three PrePFAAs (i.e., 8:2 FTSA, 8:2 FTOH and SAmPAP) in the presence of six ENMs (i.e., $nTiO_2$, nZnO, nFe_2O_3, nCuO, GO and MWCNTs) under simulated sunlight irradiation.

Fig. 3. EPR spectra of DMPO-$^{\bullet}$OH adducts in aqueous solution (a), DMPO-$O_2^{\bullet-}$adducts in methanol (b), and TEMP-$^1O_2$ adducts in aqueous solution (c) after ENMs suspensions were irradiated by simulated sunlight for 10 min. [DMPO] = 0.04 mol L^{-1}, [TEMP] = 0.04 mol L^{-1} and [ENMs]= 0.1 g L^{-1}.

Fig. 4. Concentrations of $^{\bullet}$OH, $O_2^{\bullet-}$ and $^1O_2$ generated by six ENMs (0.1 g L^{-1}) under the irradiation of simulated sunlight for 10 min, and the transformation kinetic rates of three PrePFAAs under the irradiation of simulated sunlight when coexisting with six ENMs.

Fig. 5. Concentrations of PrePFAAs photolysis products as a function of reaction time: (a–g) 8:2 FTSA, (h–n) 8:2 FTOH, and (o–u) SAmPAP. The experiments were conducted using 10 mg L^{-1} of PrePFAAs and 0.1 g L^{-1} of ENMs (i.e., $nTiO_2$, nZnO, nFe_2O_3, nCuO, GO or MWCNTs under simulated sunlight irradiation conditions.

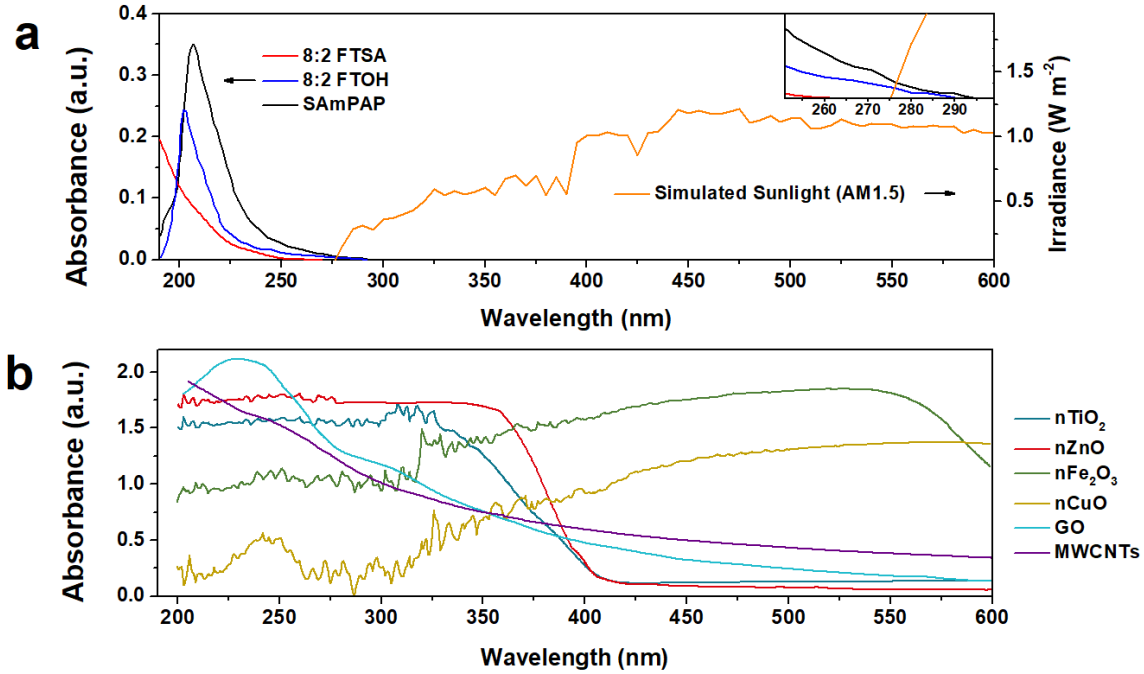

Fig. 1. (a) Molar absorptivity of 8:2 FTSA, 8:2 FTOH, SAmPAP, and emission spectra of simulated sunlight (Xenon lamp with AM 1.5G filter); (b) Diffuse reflection spectrum of six ENMs, including $nTiO_2$, nZnO, nFe_2O_3, nCuO, GO and MWCNTs.

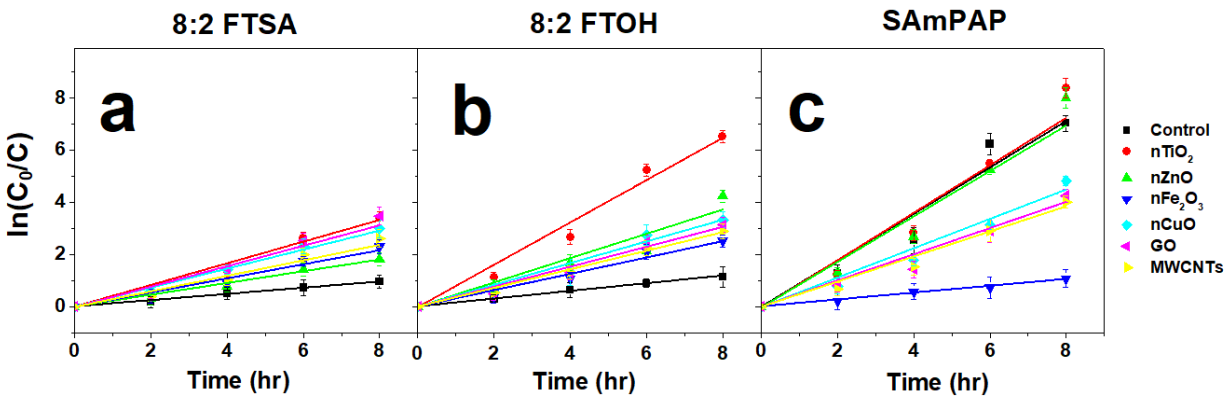

Fig. 2. Transformation kinetics of three PrePFAAs (i.e., 8:2 FTSA, 8:2 FTOH and SAmPAP) in the presence of six ENMs (i.e., $nTiO_2$, nZnO, nFe_2O_3, nCuO, GO and MWCNTs) under simulated sunlight irradiation.

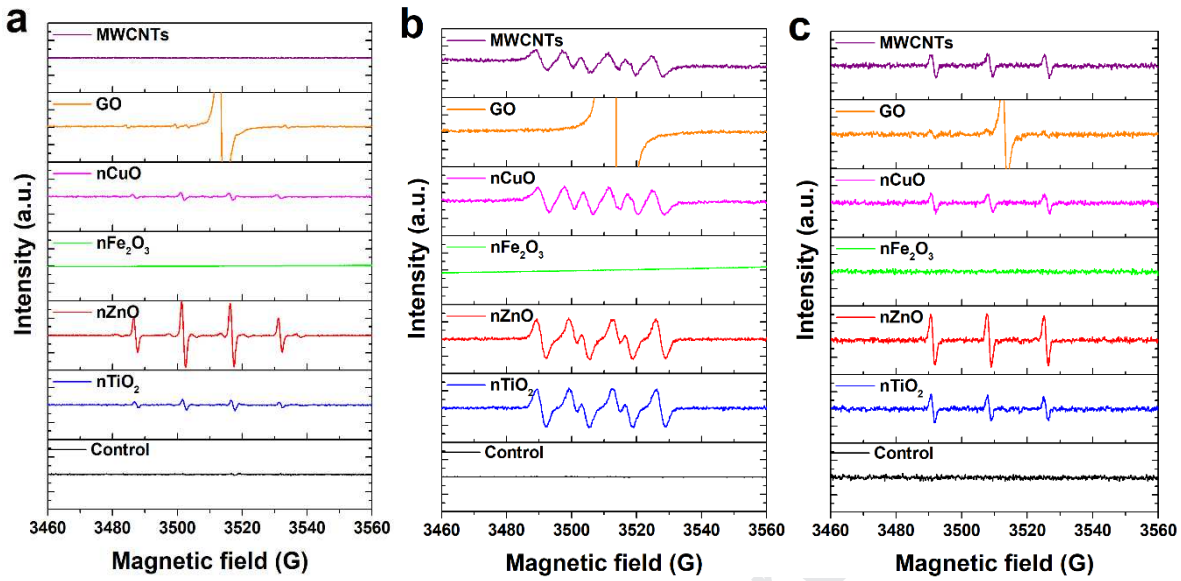

Fig. 3. EPR spectra of DMPO-$^{\bullet}$OH adducts in aqueous solution (a), DMPO-$O_2^{\bullet-}$adducts in methanol (b), and TEMP-$^1O_2$ adducts in aqueous solution (c) after ENMs suspensions were irradiated by simulated sunlight for 10 min. [DMPO] = 0.04 mol L^{-1}, [TEMP] = 0.04 mol L^{-1} and [ENMs]= 0.1 g L^{-1}.

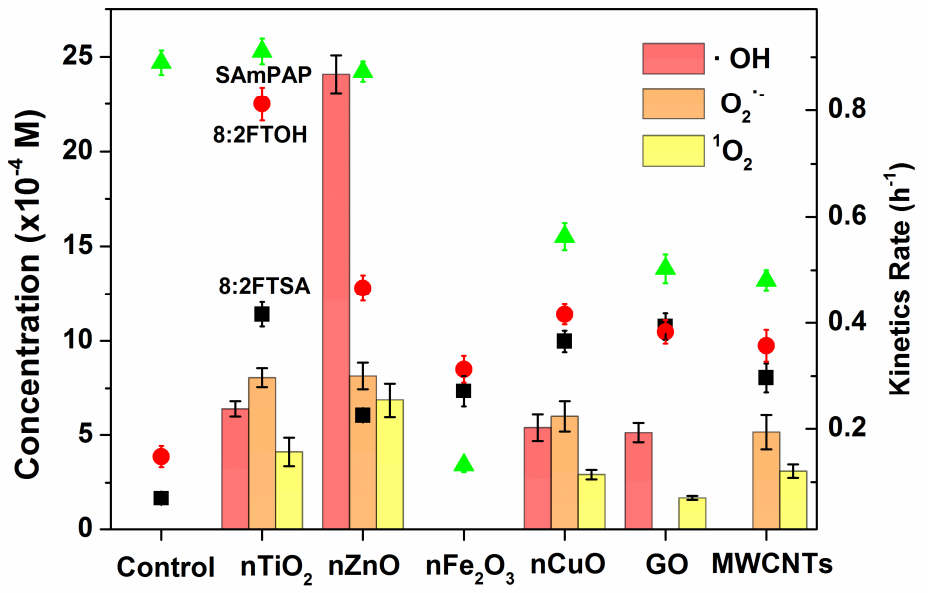

Fig. 4. Concentrations of $^{\cdot}$OH, $O_2^{\cdot-}$ and $^1O_2$ generated by six ENMs (0.1 g L^{-1}) under the irradiation of simulated sunlight for 10 min, and the transformation kinetic rates of three PrePFAAs under the irradiation of simulated sunlight when coexisting with six ENMs.

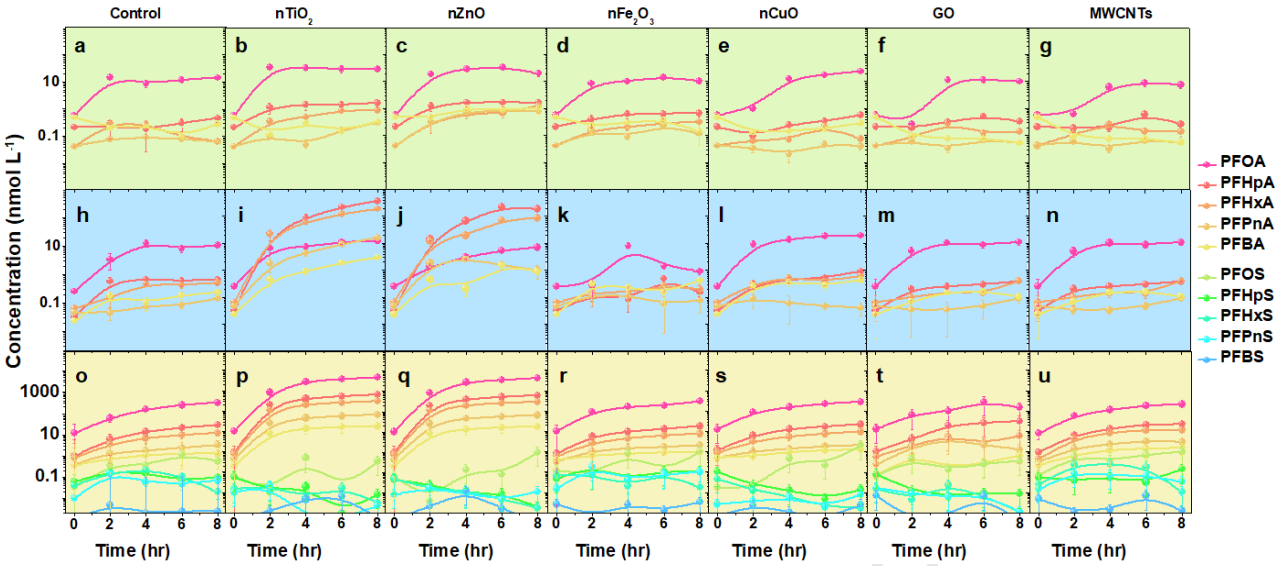

Fig. 5. Concentrations of PrePFAAs photolysis products as a function of reaction time: (a–g) 8:2 FTSA, (h–n) 8:2 FTOH, and (o–u) SAmPAP. The experiments were conducted using 10 mg L^{-1} of PrePFAAs and 0.1 g L^{-1} of ENMs (i.e., $nTiO_2$, nZnO, nFe_2O_3, nCuO, GO or MWCNTs under simulated sunlight irradiation conditions.

Highlights

- ENMs can promote or inhibit the photochemical transformation of PrePFAAs in water.
- PrePFAAs could be transformed to PFOA or/and PFOS and other shorter chain PFAAs.
- High concentrations of PFAAs products were detected in the presence of most ENMs.
- Photo-generated ROS play major roles in photochemical transformation of PrePFAAs.
- Photo-stability and photo-shielding of ENMs also affect transformation of PrePFAAs.

Declaration of interests

☒ The authors declare that they have no known competing financial interests or personal relationships that could have appeared to influence the work reported in this paper.

☐The authors declare the following financial interests/personal relationships which may be considered as potential competing interests: